Enhanced Accuracy in Respiratory Movement Detection Using Simultaneously Measured Body Proximity Signals via a Capacitive Sheet Electrode

Mikito Koyama
Department of Electrical and Electronic Engineering
Tokyo Denki University
Tokyo, Japan
24kmj16@ms.dendai.ac.jp

Akinori Ueno
Department of Electrical and Electronic Engineering
Tokyo Denki University
Tokyo, Japan
https://orcid.org/0000-0002-5710-1721

***Abstract*—The previously proposed capacitive sheet electrode enables simultaneous acquisition of electrocardiogram (ECG), respiratory movement (RM), and body proximity data. However, its RM detection accuracy remained below 85%. This study aimed to improve the detection accuracy of RM measured from the chest and abdomen during sleep using the sheet electrode placed under the bedsheet. A new detection algorithm was developed by leveraging concurrently measured body proximity signals and identifying periods of body movement. Analysis of overnight measurements from seven subjects revealed the following: (1) the mean detection accuracies of the new algorithm significantly increased ($p < 0.01$) by 6.9% for the chest and 8.8% for the abdomen, and (2) the mean accuracies reached 88.8% and 91.2%, respectively. These results demonstrate the superiority of the new algorithm.**

Keywords—respiratory movement, body proximity signal, capacitive sheet electrode

I. Introduction

Among cardiovascular diseases, the prevalence of heart failure (HF) was estimated at 60 million people worldwide in 2016 [1]. Due to an aging population, the number of HF patients in Japan is projected to reach 1.3 million by 2030 [2]. HF is rarely reversible and causes a progressive, nonlinear decline in health-related quality of life [3]. Moreover, 61.3% of hospitalized HF patients are readmitted within one year due to HF [4]. Home telemonitoring systems help reduce HF-related hospitalizations and all-cause mortality among HF patients [5]. Regarding readmissions, respiratory rate has been reported as the most significant factor in home monitoring [6]. New-onset atrial fibrillation is also linked to increased HF hospitalizations [7]. Therefore, electrocardiogram (ECG) measurement is essential for diagnosing atrial fibrillation, and simultaneous monitoring of ECG and respiratory movement (RM) is necessary to evaluate the prognosis of discharged HF patients.

During home monitoring, patients' physiological signals should be measured without disrupting daily life. To achieve this, we focused on a noncontact, in-bed measurement approach using a capacitive sheet electrode [8]. This electrode can simultaneously capture both physiological and behavioral signals, including capacitive ECG (cECG), RM, body proximity (BPx), and lying posture. Furthermore, the modified sheet electrodes achieved high detection rates (>90%) for P-wave of cECG [9], which is a predictor of atrial fibrillation onset [10]. Despite this advantage, the detection accuracy of RM during overnight (6 h) measurements remained at 82.4% for the chest and 81.9% for the abdomen [8]. As noted in [8], baseline fluctuations in the RM signal following body movements (BM) were identified as a major factor contributing to low detection accuracy. In this study, we aimed to enhance RM detection accuracy by utilizing BM information derived from simultaneously measured chest and abdominal BPx signals.

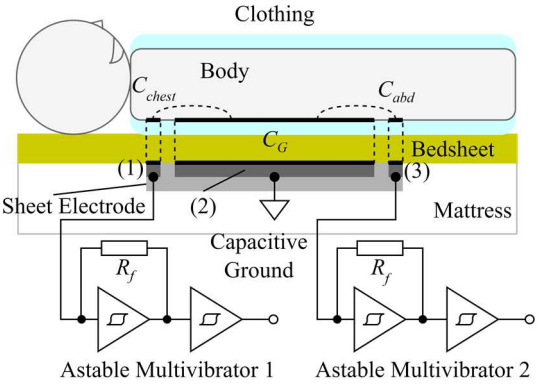

Fig. 1. Schematic of capacitive couplings related to the measurement principle of body proximity (BPx) and chest and abdominal respiratory movements (RMs).

II. Materials and Methods

A. Measurement Principle of BPx and RM

As shown in Fig. 1, the sheet electrode is placed beneath the subject's back, underneath the bed sheet. The outer electrodes (1) and (3) are positioned near the shoulder and lower back to enable independent BPx and RM measurements from the chest and abdomen. The center electrode (2) serves as a capacitive ground when coupled with the subject's trunk or upper body. It also functions as two capacitive sensors in conjunction with the outer electrodes (1) and (3). The three electrodes (1), (2), and (3) form capacitive couplings with capacitances C_{chest}, C_G, and C_{abd} to the dorsal surface of the upper body through the subject's clothing and the bedsheet.

C_{chest} and C_G are connected in series and integrated into Astable Multivibrator 1. This multivibrator oscillates at a specific frequency, $f_{osc(1)}$, which depends on the net capacitance $C_{s(1)}$ formed by the series-connected capacitors. When $C_{chest} << C_G$ in the sheet electrode, $C_{s(1)}$ can be approximated as follows:

$$C_{s(1)} = \frac{C_{chest}C_G}{C_{chest} + C_G} = \frac{C_{chest}}{1 + C_{chest}/C_G} \approx C_{chest}. \quad (1)$$

The oscillation frequency $f_{osc(1)}$ can be represented in terms of C_{chest} as follows:

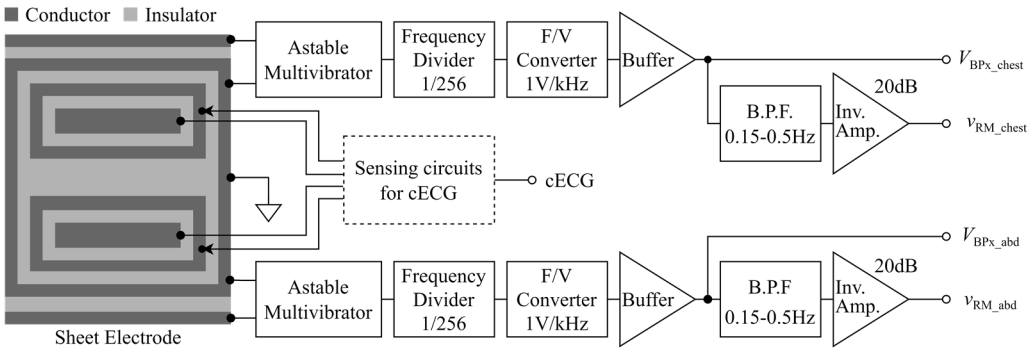

Fig. 2. Block diagram of the sensing circuits for body proximity (BPx) and chest and abdominal respiratory movement (RM) signals.

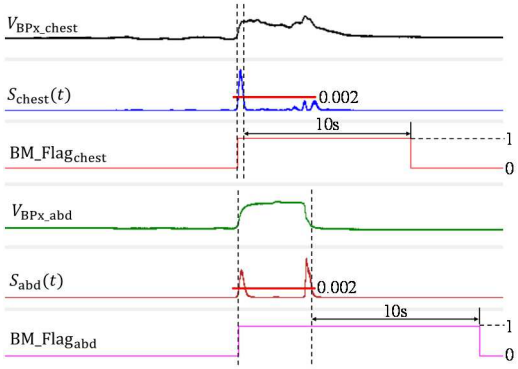

Fig. 3. Illustration of the detection algorithm for body movements (BM).

$$f_{osc(1)} = \frac{k_{osc}}{R_f C_{s(1)}} \approx \frac{k_{osc}}{R_f C_{chest}}, \quad (2)$$

where R_f is the resistance shown in Fig. 1, and k_{osc} is a constant determined by the supply voltage of the Schmitt trigger inverter.

As shown in Fig. 2, the output signal of the astable multivibrator is passed through a 1/256 frequency divider and then input to a frequency-to-voltage (F/V) converter. The output voltage V_{out_chest} of the F/V converter is proportional to $f_{osc(1)}/256$, as follows:

$$V_{BPx\_chest} = k_{fv} \frac{f_{osc(1)}}{256} \approx \frac{k_{fv} k_{osc}}{256 R_f C_{chest}}. \quad (3)$$

However, k_{fv} is a constant determined by the resistance and capacitance within the F/V converter. C_{chest} is defined by the dielectric constant ε [F·m], the area of the coupling region A_{chest} [m^2], and the coupling distance d_{chest} [m]. This coupling distance is the sum of two time-varying components: $d_{BPx(1)}$ and $\Delta d_{RM(1)}$. Specifically, C_{chest} is calculated as follows:

$$C_{chest} = \varepsilon \frac{A_{chest}}{d_{chest}} = \varepsilon \frac{A_{chest}}{d_{BPx(1)} + \Delta d_{RM(1)}}. \quad (4)$$

Where $d_{BPx(1)}$ is the distance between the subject's upper body and electrode (1), and $\Delta d_{RM(1)}$ represents the variation in coupling distance caused by RM. By substituting (4) into (3), we obtain:

$$V_{BPx\_chest} = \frac{k_{fv} k_{osc}}{256 R_f \varepsilon} \cdot \frac{d_{BPx(1)} + \Delta d_{RM(1)}}{A_{chest}}. \quad (5)$$

Note that in (5), $d_{BPx(1)}$ represents the distance between the shoulder and outer electrode (1) and is thus a fixed value for a subject in a lying posture. When the subject shifts into or out of a lateral position, the change in $1/A_{chest}$ becomes the dominant factor affecting $d_{BPx(1)} + \Delta d_{RM(1)}$. As a result, V_{BPx_chest} reflects both lying posture and BM around the chest. Meanwhile, when a subject remains stationary in a single body position, $d_{BPx(1)}$ and A_{chest} can be considered constant. In this case, the change in V_{BPx_chest} includes a time-varying small signal that reflects $\Delta d_{RM(1)}$, and it can be expressed as follows:

$$\Delta V_{BPx\_chest} = \frac{k_{fv} k_{osc}}{256 R_f \varepsilon A_{chest}} \cdot \Delta d_{RM(1)} \coloneqq v_{RM\_chest}. \quad (6)$$

In this paper, RM_{chest} was obtained by extracting the signal (v_{RM_chest}) containing the corresponding frequency components from V_{out_chest}. By considering the series-connected capacitors C_{abd} and C_G in Fig. 1, we can similarly derive V_{BPx_abd} and v_{RM_abd}, which are sensitive to BPx_{abd} and RM_{abd}, respectively, at the abdomen.

B. Detection Algorithm for BM and RM

Detection of BM was performed prior to RM detection, following the algorithm described in [11]. RMs of the chest and abdomen were detected from the v_{RM_chest} and v_{RM_abd} signals, respectively, in combination with BM_Flag_{chest} and BM_Flag_{abd}, which indicate BM of the chest and abdomen estimated from V_{BPx_chest} and V_{BPx_abd} signals. BM of the chest and abdomen were determined as follows: first, the mean values ($M_{chest}(t)$ and $M_{abd}(t)$) of $V_{BPx\_chest}(t)$ and $V_{BPx\_abd}(t)$ at time t were calculated over the previous 0.45 s. Then, the squared differences ($S_{chest}(t)$ and $S_{abd}(t)$) between the means and the current voltages $V_{BPx\_chest}(t)$ and $V_{BPx\_abd}(t)$ were computed. As shown in Fig. 3, when $S_{chest}(t)$ or $S_{abd}(t)$ exceeded a threshold (0.002), BM_Flag_{chest} or BM_Flag_{abd} was set to 1. Each flag then returned to 0 when 10 s had passed since $S_{chest}(t)$ or $S_{abd}(t)$ fell below the threshold.

The peaks and troughs of RM in the chest and abdomen were detected from v_{RM_chest} and v_{RM_abd}, respectively, within segments where both BM_Flag_{chest} and BM_Flag_{abd} were "0" (Fig. 4). As shown in Fig. 5, the detection time window was set to $t \pm 0.8$ s. When $v_{RM}(t)$ was greater than or equal to a positive threshold (V_{h+}) and was the maximum value within the window, the maximum at time t was considered a peak candidate of RM (inhalation). Furthermore, if the time difference Δt_s between the previous and current zero-crossing points exceeded 1.0 s, the candidate was confirmed as a peak, and $p(t)$ was set to "1." Similarly, troughs of RM were detected, and $p(t)$ was set to "−1" for the chest and abdomen.

C. Analytical Data

As shown in Fig. 6, BPx, RM, and cECG signals were simultaneously recorded during 6-h sleep sessions from seven male subjects (20–23 years old, 1.60–1.87 m height, 55.0–78.8 kg weight, 20.9–26.6 kg/m^2 BMI). The participants wore

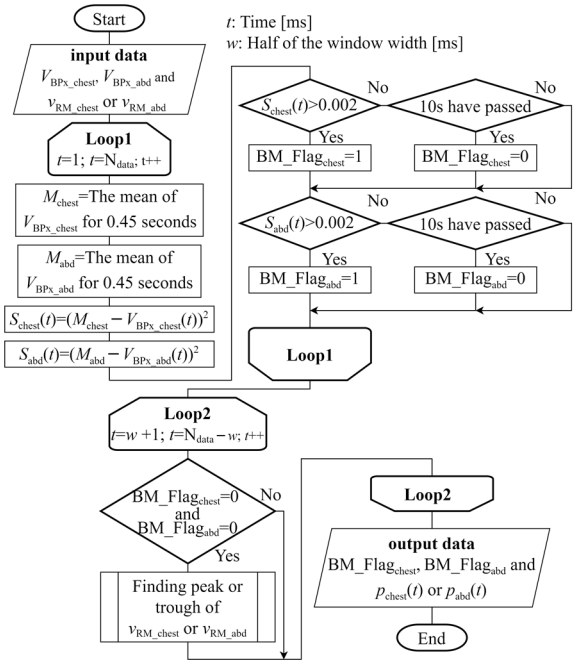

Fig. 4. Flowchart for identifying non-analysis segments in chest and abdominal respiratory movement (RM) signals.

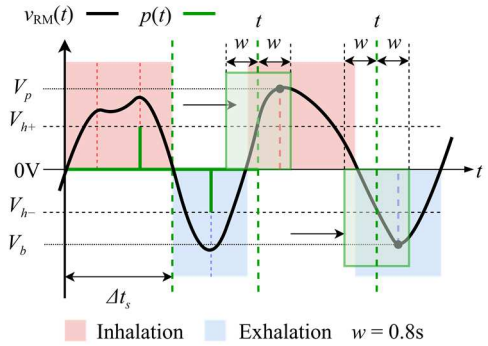

Fig. 5. Illustration of the detection algorithm for inhalation and exhalation phases.

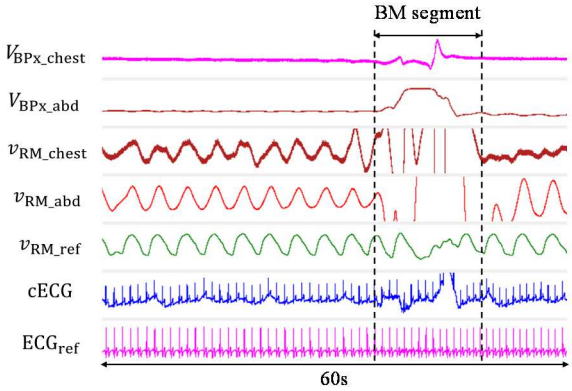

Fig. 6. Simultaneous measurement waveforms of body proximity (BPx), respiratory movements (RMs), and electrocardiogram (ECG) in subject #4.

0.36 mm-thick cotton nightwear and lay on a 0.33 mm-thick cotton bedsheet placed over the sheet electrode in a free lying position (see [8]). All subjects reported no history of cardiopulmonary or cardiovascular disease and provided informed consent. All experimental procedures were approved in advance by the Human Life Ethics Committee of Tokyo Denki University. Reference signals for RM (RM_{ref}) and ECG (ECG_{ref}) were simultaneously obtained using a commercially available telemetry system (BN-RSPEC, BIOPAC Systems). A commercial belt-type transducer was wrapped around the abdomen for RM_{ref} measurement. All signals obtained by the capacitive and reference systems were synchronously digitized at 1 kHz with 16-bit resolution.

D. Evaluation of the Proposed Algorithm

All RM_{chest}, RM_{abd}, and RM_{ref} signals obtained during the six-hour sleep sessions were preprocessed using a second-order digital band-pass filter (IIR, 0.15–0.5 Hz). The filtered signals were then analyzed using the proposed algorithm described in Section II-B. When the detected peak or trough of RM_{chest} or RM_{abd} occurred within ±2.0 s of the corresponding peak or trough of RM_{ref}, inhalation or exhalation was considered correctly detected. Conversely, if the RM_{chest} or RM_{abd} peak or trough did not fall within ±2.0 s of RM_{ref}, it was regarded as a false detection. If no corresponding peak or trough was detected in RM_{chest} or RM_{abd}, the RM_{ref} event was considered undetected. Based on the detection results, sensitivity (P_{SNS}), accuracy (P_{ACC}), and positive predictive value (P_{PPV}) were calculated for the RM_{chest} and RM_{abd} measurements, respectively. To evaluate the proposed detection algorithm, these three detection rates (P_{SNS}, P_{ACC}, and P_{PPV}) were also computed using the conventional detection algorithm reported in [8]. Test of normality and paired t-test were performed using a commercial software (JMP, Statistical Discovery) for them.

III. Results and Discussion

As shown in Fig. 7, the mean detection rates (P_{SNS}, P_{ACC}, and P_{SNS}) achieved by the proposed algorithm were significantly higher than those of the conventional algorithm for both RM_{chest} and RM_{abd}, respectively. In the proposed algorithm, all rates except P_{ACC} for RM_{chest} exceeded 90%. As shown individually in Table I, P_{ACC} from the proposed algorithm was higher across all subjects for both RM_{chest} and RM_{abd}. This improvement can be partially attributed to the use of BPx signals for detecting BM. Thus, we hypothesized that by distinguishing large inhalation movements from BM using BPx signals, the proposed algorithm may reduce the number of false detections. As a result, this classification effectively suppressed the sharp increase in threshold voltage that was previously caused by false detections.

Another reason for the superiority of the proposed algorithm lies in the introduction of dual detection of both peaks and troughs (i.e., inhalation and exhalation) for each RM signal. In the conventional algorithm [8], only a single zero-crossing point was detected for each RM_{chest} and RM_{abd}, respectively. As a result, subtle fluctuations in the respiratory phase could lead to small differences in zero-crossing timing between RM_{chest} and RM_{ref}, or RM_{abd} and RM_{ref}, increasing the likelihood of falsely detected or undetected respiratory movements. In contrast, the proposed algorithm identifies two distinct feature points peak and trough corresponding to inhalation and exhalation for each RM_{chest} and RM_{abd}. This dual detection approach enables greater robustness against phase fluctuations and is thus considered to improve overall detection accuracy. While not yet being performed, the proposed algorithm can compute the amplitudes of each respiration. Therefore, further analysis of respiration amplitude would be beneficial to evaluate breathing dynamics.

Focusing on the number of reference data (N_{TP}+N_{FN}) for subjects #3 and #6 in Table I, and comparing them between the "Conv × 2" and "Pro" methods, the proposed method

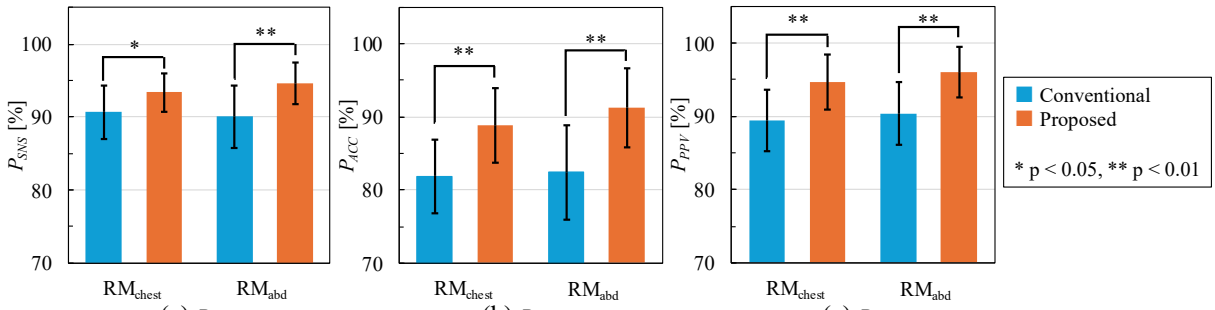

(a) P_{SNS} (b) P_{ACC} (c) P_{PPV}

Fig. 7. Comparison of (a) sensitivity (P_{SNS}), (b) accuracy (P_{ACC}), and (c) positive predictive value (P_{PPV}) of chest and abdominal respiratory movement (RM) signals between the conventional and proposed algorithms.

TABLE I. SENSITIVITY (P_{SNS}), ACCURACY (P_{ACC}), POSITIVE PREDICTIVE VALUE (P_{PPV}), AND NUMBER OF REFERENCE DATA (TRUE POSITIVES PLUS FALSE NEGATIVES, N_{TP}+N_{FN}) FOR INHALATION AND EXHALATION IN THE CHEST AND ABDOMEN FOR EACH SUBJECT.

Subject ID	Chest								Abdomen							
	P_{SNS} [%]		P_{ACC} [%]		P_{PPV} [%]		N_{TP}+N_{FN} (True Events)		P_{SNS} [%]		P_{ACC} [%]		P_{PPV} [%]		N_{TP}+N_{FN} (True Events)	
	Conv	Pro	Conv	Pro	Conv	Pro	Conv × 2	Pro	Conv	Pro	Conv	Pro	Conv	Pro	Conv × 2	Pro
#1	93.6	94.8	86.6	88.8	92.0	93.3	8770	8187	92.2	95.1	82.4	89.7	88.5	94.0	8770	8187
#2	90.9	92.6	84.7	92.1	92.6	99.4	11858	11409	88.1	93.8	77.8	92.9	87.0	99.0	11858	11409
#3	92.5	96.8	82.4	94.5	88.3	97.5	10848	8845	96.1	97.9	91.6	96.7	95.1	98.7	10848	8845
#4	89.4	94.1	79.9	90.9	88.3	96.4	11046	10416	87.8	97.2	79.9	96.6	89.9	99.3	11046	10416
#5	82.4	88.3	73.9	79.2	87.8	88.5	8938	8768	82.4	89.6	75.5	81.2	90.0	89.7	8938	8768
#6	92.8	91.6	76.5	83.4	81.3	90.3	9910	7610	89.9	92.0	77.1	86.1	84.4	93.1	9910	7609
#7	93.1	95.5	89.1	93.0	95.4	97.3	10790	9917	94.4	97.2	92.4	95.4	97.7	98.1	10790	9917
Mean	90.7	93.4	81.9	88.8	89.4	94.7	10309	9307	90.1	94.7	82.4	91.2	90.4	96.0	10309	9307
SD	±3.6	±2.6	±5.0	±5.2	±4.2	±3.8	±1060	±1234	±4.3	±2.9	±6.4	±5.4	±4.3	±3.5	±1060	±1234

Conv: Conventional, Pro: Proposed

yielded approximately 2000 fewer data points that indicated nearly double the reference count using the conventional method. This difference is likely due to the exclusion of time segments in which either BM_Flag$_{chest}$ or BM_Flag$_{abd}$ was set to "1" from the analysis. As in [8], BPx signals can be used to classify lying postures with accuracy over 90%. Thus, adjustive thresholds based on this may allow more accurate detection for irregular respiration with large amplitude.

IV. CONCLUSION AND FUTURE WORKS

In this study, we aimed to enhance the accuracy of respiratory movement detection by incorporating simultaneously measured body proximity signals. In seven subjects, the proposed algorithm achieved a mean detection accuracy of 88.8% for the chest and 91.2% for the abdomen, significantly surpassing the performance of the conventional algorithm ($p < 0.01$). However, some false detections were observed during body movement recognition. Appropriate threshold settings are crucial for maintaining the reliability of the body movement detection algorithm. As for future work, it is necessary to expand the size of participants, including people with chronic HF and different physical characteristics.

REFERENCES

[1] T. Vos, A. A. Abajobir, C. Abbafati, K. M. Abbas, K. H. Abate, et al., "Global, regional, and national incidence, prevalence, and years lived with disability for 328 diseases and injuries for 195 countries, 1990-2016: a systematic analysis for the global burden of disease study 2016," Lancet, vol. 390, pp. 1211–1259, 2017.

[2] Y. Okura, M. M. Ramadan, Y. Ohno, W. Mitsuma, K. Tanaka, et al., "Impending epidemic: future projection of heart failure in Japan to the year 2055," Circ. J., vol. 72, pp. 489–491, 2008.

[3] L. A. Allen, L. W. Stevenson, K. L. Grady, N. E. Goldstein, D. D. Matlock, et al., "Decision making in advanced heart failure: a scientific statement from the american heart association," Circulation, vol. 125, pp. 1928–1952, 2012.

[4] S. Chun, J. V. Tu, H. C. Wijeysundera, P. C. Austin, X. Wang, et al, "Lifetime analysis of hospitalizations and survival of patients newly admitted with heart failure," Circ. Heart Fail., vol. 5, pp. 414–421, 2012.

[5] N. T. B. Scholte, M. T. Gürgöze, D. Aydin, D. A. M. J. Theuns, O. C. Manintveld et al., "Telemonitoring for heart failure: a meta-analysisi," Eur. Heart J., vol. 44, pp. 2911–2926, 2023.

[6] M. K. Bennett, M. Shao and E. Z. Gorodeski, "Home monitoring of heart failure patients at risk for hospital readmission using a novel under-the-mattress piezoelectric sensor: a preliminary single centre experience," J. Telemed. Telecare, vol. 23, pp. 60–67, 2017.

[7] T. Yamauchi, Y. Sakata, M. Miura, T. Onose, K. Tsuji, et al., "Prognostic impact of atrial fibllation and new risk score of its onset in patients at high risk of heart failure," Circ. J., vol. 81, pp. 185–194, 2017.

[8] M. Takano and A. Ueno, "Noncontact in-bed measurements of physiological and behavioral signals using an integrated fabric-sheet sensing scheme," IEEE J. Biomed. Health Inform., vol. 23, pp. 618–630, Mar. 2019.

[9] I. Kudo and A. Ueno, "Evaluation of P-wave detection capability of capacitive electrocardiogram measurement system with electrode sheet," in 2024 IEEE 20th Conference on Body Sensor Networks (BSN, Chicago), Oct. 2024.

[10] F. Kreimer, A. Aweimer, A. Pflaumbaum, A. Mügge, M. Gotzmann, "Impact of P-wave indices in prediction of atrial fibrillation—Insight from loop recorder analysis ", Ann. Noninvasive. Electrocardiol., vol. 26, no. 5, e12854, 2021.

[11] Y. Sato and A. Ueno, "Bed-exiting behavior detection in sheeting IoT system with printed electrode," in 2024 IEEE 20th Conference on Body Sensor Networks (BSN, Chicago), Oct. 2024.